JMEPEG (2010) 19:921–927
DOI: 10.1007/s11665-009-9575-7

1059-9495/$19.00

Stress-Strain Behaviors Simulation of High Chromium Steel at Elevated Temperatures

Ligang Liu, Qiang Li, Bo Liao, Yukui Gao, Yuhui Wang, Xuejun Ren, and Qingxiang Yang

(Submitted March 26, 2009; in revised form September 29, 2009)

It is important but difficult to study the constitutive equations describing the mechanical properties of steels. In this work, a thermal/mechanical simulator was used in conjunction with the Anand model to obtain the stress-strain curves for a high chromium steel associated with different temperature/strain rate pairs. The finite element software, ANSYS, was used to simulate the stress-strain behavior of a high chromium steel during casting at the strain rates of 1, 0.1, and 0.01 1/s, and to validate the Anand model. The results show that the high-temperature deformation is mainly plastic and the von Mises stresses are small, the stresses introduced at elevated temperatures have little effect on the residual stress fields, and the simulation of the mechanical behavior of steels using an elastic-plastic model at low temperatures during cooling is acceptable.

Keywords Anand model, casting, FEM, numerical simulation, strain, stress

1. Introduction

The study of deformation mechanisms and failure are important research topics for mechanical and materials engineers (Ref 1-4). At elevated temperatures, the strength of materials is low and inhomogeneous deformation usually occurs. To understand the mechanical behaviors of workpieces at elevated temperatures, constitutive equations of the corresponding materials should be established (Ref 5-8). An application of this is centrifugal casting in which liquid metal is poured into a rotating preheated mold, followed by cooling, crystallization, and solidification under centrifugal force. Centrifugal casting has the characteristics of compact structures, less stomata, less shrinkage cavities, and impurities. However, when workpieces are solidified, inhomogeneous deformation and internal stress exist in workpieces under the effects of the centrifugal force and thermal stresses result from temperature gradient during casting process. It is difficult to observe the evolution of the internal stress field in the rotating workpieces at elevated temperatures.

Ligang Liu, National Key Laboratory of Metastable Materials Science & Technology, College of Material Science and Engineering, Yanshan University, Qinhuangdao 066004, P.R. China and College of Mechanical Engineering, Yanshan University, Qinhuangdao 066004, P.R. China; **Qiang Li, Bo Liao, Yuhui Wang,** and **Qingxiang Yang**, National Key Laboratory of Metastable Materials Science & Technology, College of Material Science and Engineering, Yanshan University, Qinhuangdao 066004, P.R. China; **Yukui Gao**, Beijing Institute of Aeronautical Materials, Beijing 100095, P.R. China; and **Xuejun Ren**, School of Engineering, Liverpool John Moores University, Liverpool L3 3AF, UK. Contact e-mails: yqxsyfys@yahoo.com, qxyang@ysu.edu.cn and llgysu@sogou.com.

Numerical simulations have advantages over experiments in studying the physical phenomena that are difficult to measure under extreme conditions. For example, numerical simulations of the stress fields of rollers are very important, which are helpful to predict hot crack, cold crack, and deformation. The bases of thermal stress analyses during casting process are the numerical simulations of temperature fields, which are basically mature (Ref 1, 7-16). The stress simulation of solidified ingot shells was first performed by using analytical method in 1960s. Since then, stress field simulations have developed rapidly. However, there are few studies emphasizing the stress-strain behaviors of casting at elevated temperatures.

In order to understand the stress evolution of castings during centrifugal casting process directly and optimize casting technologies in both theory and practice, the temperature of the high chromium steel-nodular cast iron steel clad roll during casting process and the stress field of the high chromium steel after mold filling process at elevated temperatures were simulated by using FEM. Unified viscoplastic Anand model was used to describe the constitutive behaviors at elevated temperatures. The parameters of Anand model were determined by analyzing experimental stress-strain data.

2. Anand Model Summary

Thermodynamic behaviors of metals are complex at elevated temperatures. The kinetics of deformation is highly dependent on temperature and strain rate. During such process, microstructure evolution produces strain-hardening, dynamic recovery, and in many instances dynamic recrystallization. Anand model is a single-scalar internal variable model proposed by Anand (Ref 17) and Anand and Brown (Ref 19) for isotropic large deformation with small elastic deformation (Ref 17-19). This elasto-viscoplastic model has two significant characteristics: (1) there is no yield surface in stress space. The loading and unloading rules are not needed during loading and unloading processes; (2) a single-scalar internal variable (deformation resistance *s*) is used to describe average resistance of macroscopic plastic flow induced by internal isotropic hardening, which is related with dislocation density, solid-solution strengthening, and grain size effect.

Deformation resistance s is proportional to equivalent stress σ,

$$\sigma = cs \qquad c < 1, \tag{Eq 1}$$

where c is a material parameter, as a function of strain rate:

$$c = \frac{1}{\xi}\sinh^{-1}\left[\left(\frac{\dot{\varepsilon}_p}{A}\exp\left(\frac{Q}{RT}\right)\right)^m\right], \tag{Eq 2}$$

where $\dot{\varepsilon}_p$, A, Q, m, ξ, R, and T are inelastic strain rate, pre-exponential factor (a constant determined by experiment), activation energy, strain rate sensitivity, stress intensity factor, gas constant, and temperature, respectively.

The flow equation of Anand model can be described according to hyperbolic creep rule as:

$$\dot{\varepsilon}_p = A\exp\left(-\frac{Q}{RT}\right)\left[\sinh\left(\xi\frac{\sigma}{s}\right)\right]^{1/m}. \tag{Eq 3}$$

The steady plastic flow of Anand model can be described as below:

$$\dot{\varepsilon}_p = \dot{\varepsilon} = A\exp\left(-\frac{Q}{RT}\right)\left[\sinh\left(\xi\frac{\sigma^*}{s^*}\right)\right]^{1/m}. \tag{Eq 4}$$

The saturated stress can be derived from the above formula,

$$\sigma^* = cs^* = \frac{\hat{s}}{\xi}\left(\frac{\dot{\varepsilon}_p}{A}\exp\left(\frac{Q}{RT}\right)\right)^n \sinh^{-1}\left[\left(\frac{\dot{\varepsilon}_p}{A}\exp\left(\frac{Q}{RT}\right)\right)^m\right]. \tag{Eq 5}$$

The internal evolution equation can be expressed as:

$$\dot{s} = \left[h_0\left|1-\frac{s}{s^*}\right|^a \cdot \mathrm{sign}\left(1-\frac{s}{s^*}\right)\right]\cdot\dot{\varepsilon}_p, \quad a \geq 1, \tag{Eq 6}$$

where

$$s^* = \hat{s}\left[\frac{\dot{\varepsilon}_p}{A}\exp\left(\frac{Q}{RT}\right)\right]^n. \tag{Eq 7}$$

In those above functions, h_0 and a are the strain-hardening constant and hardening/softening strain rate sensitive coefficient, respectively. s^* represents a saturated value of s at different temperature and strain rate, $\hat{s}$ and n are the saturated coefficient of deformation resistance and strain rate sensitive coefficient of saturated deformation resistance, respectively (Ref 18, 19).

For isothermal, constant true strain rate tests were $\sigma^* = cs^*$.

$$\sigma = \sigma^* - \left[(\sigma^* - cs_0)^{(1-a)} + (a-1)\{(ch_0)(\sigma^*)^{-a}\}\varepsilon^p\right]^{1/(1-a)}. \tag{Eq 8}$$

It can be seen that there are nine material parameters in Anand viscoplastic constitutive equation, A, Q, ξ, m, n, h_0, $\hat{s}$, a, and s_0 (initial deformation resistance). During the cooling process after filling process, the internal damage and texture in high chromium can be ignored in the high chromium steel, which can be treated as isothermal. Although the use of a single-scalar internal variable limits the constitutive equations to describing the deformation behavior of initially isotropic metals up to deformation levels where significant internal damage and texture has not developed, the constitutive equations are useful for obtaining an improved analysis of various hot deformation operations of metals. Then in this work, the Anand model was used to describe the mechanical behavior of high chromium steel at elevated temperatures under the effect of the centrifugal force.

3. Experimental and Simulation Methods

In this work, the surface layer of the compound roller was high chromium steel and the core was nodular cast iron. The chemical composition (wt.%) of the high chromium steel is 1.2-1.8C, 9-15Cr, 1.0-1.5Ni, 0.1-0.4 Mo, and remainder Fe, while the chemical composition (wt.%) of the nodular cast iron is 2.7-3.2C, 1.7-2.5Si, ≤0.15P, ≤0.2S, and remainder Fe. The saturated stresses at different temperature and strain rate were measured by using Gleeble-3500 thermal/mechanical simulator. The specimens with the dimensions of φ 8 mm × 12 mm were compressed at 1150, 1200, and 1250 °C, while the strain rates range from 0.001 to 10 1/s. The measured stress-strain curves are displayed in Fig. 1. The measured results of the saturated stresses are listed in Table 1. Values of the Anand model parameters for high chromium steel were determined by following the procedure outlined below (Ref 17-19):

(1) The value of the saturation stress σ^* is determined for each test from steady state value reached in the (σ, ε) data.
(2) The values of A, Q, m, n, and the combined term of (ξ/s^*) are then determined by a nonlinear least squared fit to temperature, strain rate, and saturation stress.
(3) By using the values of A, Q, and m determined above, the value of the parameter ξ is selected such that the constant c in Eq 2 is less than unity for each test, then $\hat{s}$ is determined from the combined term (ξ/s^*).
(4) ch_0, a, and cs_0 are determined by a least squares fit of the (σ, ε) data to the integrated stress-strain relation equation (8). a is determined as the average of the values determined from each individual test. After the value of a is fixed, the least squares fit of Eq 8 to determine the final values of ch_0 and cs_0. c is determined in step (3), the h_0 and s_0 can be obtained.
(5) The value of h_0 is then obtained as the simple average:

$$h_0 = \frac{\sum_{i=1}^{q}([ch_0]_i/c_i)}{q}, \tag{Eq 9}$$

where $[ch_0]_i$ is the value of ch_0 determined in step (4) for test i, c_i is the corresponding value of c and q is the number of tests.
(6) s_0 is determined as the average of the values of s_0 determined from each individual test.

The determined parameters of Anand model are listed in Table 2.

The stress-strain curves were simulated based on Anand model by using ANSYS software and the element type is VISCO106 (2D-4 nodes). The simulation model named as M1 is shown in Fig. 2(a) and the dimensions of the model are the same as the ones used in the actual compression specimens. There are 120 elements and 143 nodes in the model. Axisymmetric constraints are applied on the nodes at the bottom boundary, and the symmetry axis is *Y*-axis. The left boundary is on the symmetry axis, and the displacement of the nodes on the left boundary along *X*-axis direction is zero, $\partial U/\partial x = 0$, in which U is displacement. The displacement along *X*-axis is coupled on the nodes at the right boundary. The displacement loading is applied on the nodes at the top boundary with the value of 4.8 cm. To investigate the mesh dependence of this model, another model named as M2 with 225 elements and 256 nodes was built shown in Fig. 2(b). The simulated stress-stain curves at the strain rates of 1 and 0.01 1/s at 1250 °C are shown in Fig. 3. It can be seen from Fig. 3 that the model used to simulate stress-strain curves is not mesh dependent. The reason is that the shape of the model is simple and the sectional dimension does not change. For verifying the correctness of the parameters of Anand model presented in this work, stress-strain curves at different true strain rates at 1200 and 1250 °C were simulated and the results were shown in Fig. 4. It can be seen from Fig. 4 that, using the chosen parameters, the simulated behaviors fit well with the experimental data.

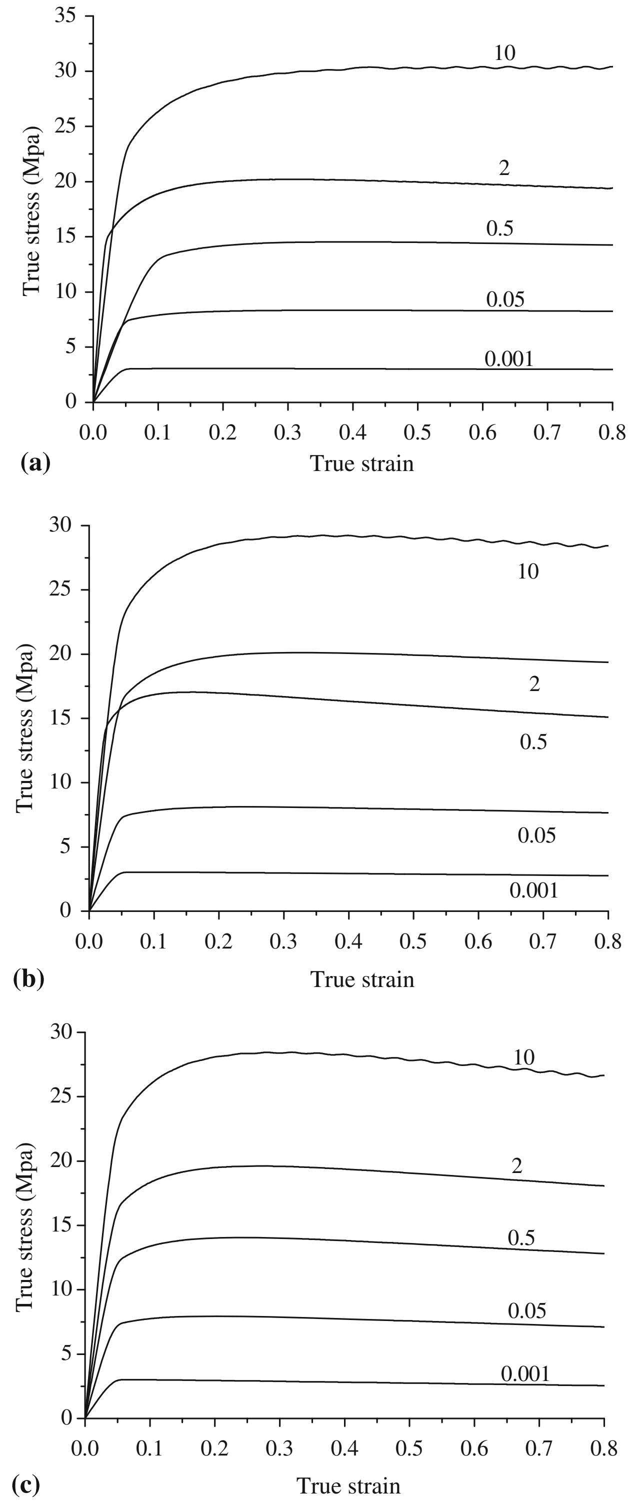

Fig. 1 Stress-strain curves at (a) 1150 °C, (b) 1200 °C, and (c) 1250 °C

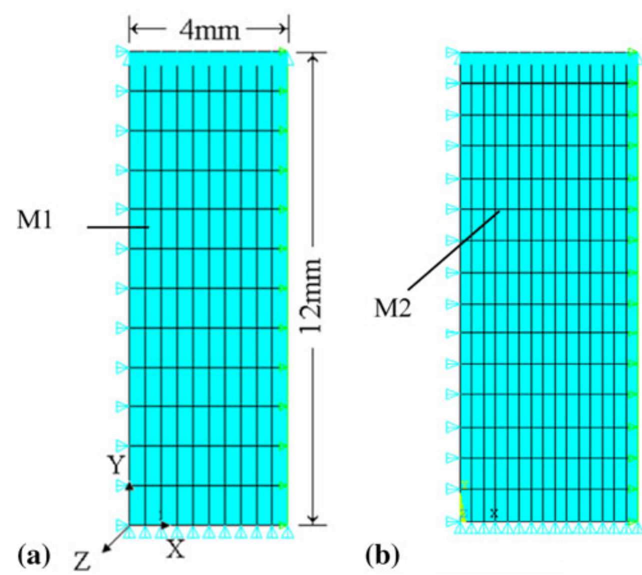

Fig. 2 Simulation model of stress-strain curves

Table 1 Values of saturated stress

	Strain rates, 1/s				
***T*, °C**	**10**	**2**	**0.5**	**0.05**	**0.001**
1150	30.3	20.2	...	8.4	3.1
1200	29.2	20.1	17.1	8.1	3
1250	28.4	19.6	14	8	3

Table 2 Parameters of Anand model

***Q*, J/mol**	***A*, 1/s**	ξ	$\hat{s}$**, MPa**	***m***	***n***	***a***	h_0**, MPa**	s_0**, MPa**
3.12e3	6.35e11	3.25	125.1	0.1956	6.869e-2	1.5	3093	61

To study the stress-strain behaviors of the high chromium steel-nodular cast iron roll during centrifugal casting process, the temperature evolution of the creep model must be determined. Thus, the temperature field of casting process was simulated first. The model of the temperature simulation is shown in Fig. 5 and the distortion ratio of height to width is 2. The element type for this simulation was PLANE55 (four nodes). The thermophysical parameters employed in temperature field simulation are listed in Table 3-5. The body dimensions of the high chromium steel-nodular cast iron steel clad roll was φ 835 mm × 2740 mm: the thicknesses of the high chromium steel layer, the primary nodular cast iron core, the secondary nodular cast iron core, the coating and the cold mold were 80, 30, 307.5, 3, and 195 mm, respectively. The total height of the simulated roller was 6070 mm. It was assumed that the mold filling process was finished immediately. The preheating temperature of the coating was 140 °C. First, the high chromium layer was poured. The casting temperature of the high chromium layer was 1425 °C. The primary nodular cast iron core was poured at 810 s, and the casting temperature was 1520 °C. The rotating speed of the centrifugal machine with value of 600 rpm was not changed during casting process and the surface convective heat transfer coefficient was 35 W/(m^2 · K). The centrifugal machine was stopped at 1600 s and the secondary nodular cast iron core was poured. Then, the surface convective heat transfer coefficient was changed from 35 to 9 W/(m^2 · K).

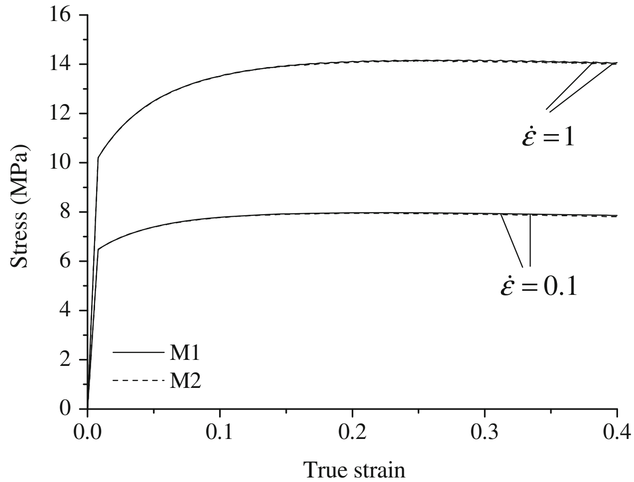

Fig. 3 Comparison of the simulated stress-strain curves between M1 and M2 shown in Fig. 2

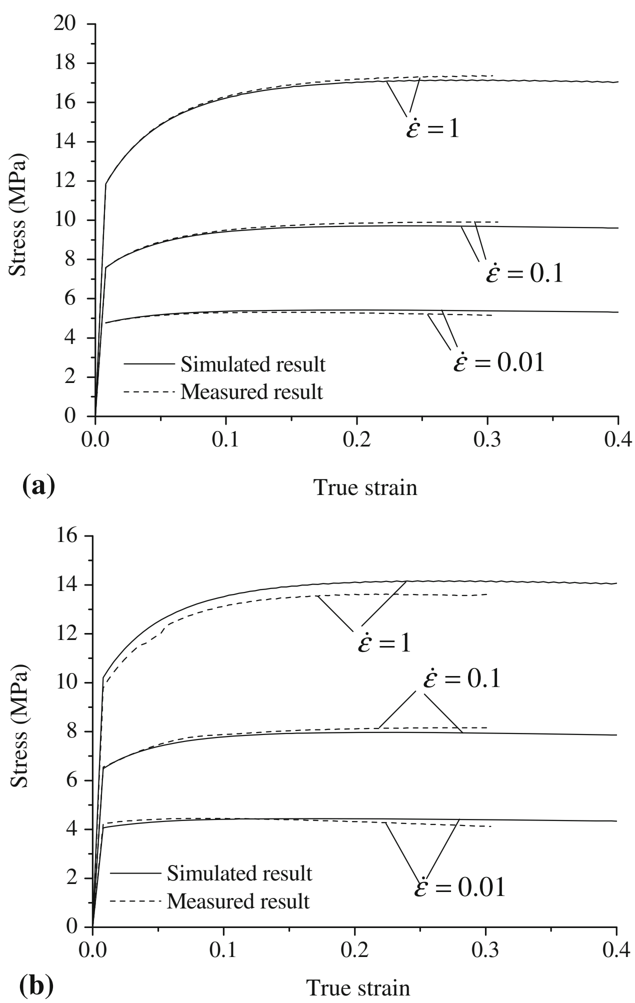

Fig. 4 Simulated and measured results of stress-strain curves at different strain rates at (a) 1200 °C and (b) 1250 °C

Then, the stress field simulation during cooling process after mold filling was performed. To simplify the stress simulation, the bottom part of the high chromium steel in Fig. 5 was selected as the stress simulation model (with the dimensions of 80 mm × 50 mm) shown in Fig. 6 and the element type was VISCO106. Based on the isotropic hypothesis, the selected elastic modulus, poisson ratio, and linear expansion coefficient

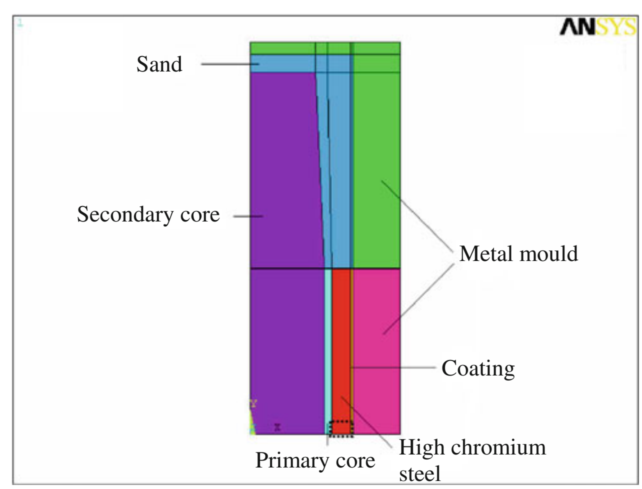

Fig. 5 Temperature field simulation model

Table 3 Thermal physical properties of the metal mold and coating

Items	ρ, kg/m^3	*C*, J/kg · °C	λ, W/m^2 · °C
Metal mold	7100	320	35
Coating	200	230	0.5
Sand	1360	1070	0.967

of the high chromium steel at elevated temperatures were 1.2×10^{11} Pa, 0.28, and 1.12×10^{-5}/°C, respectively. The rotating speed was 600 rpm, and the acceleration of gravity was 9.78 m/s^2.

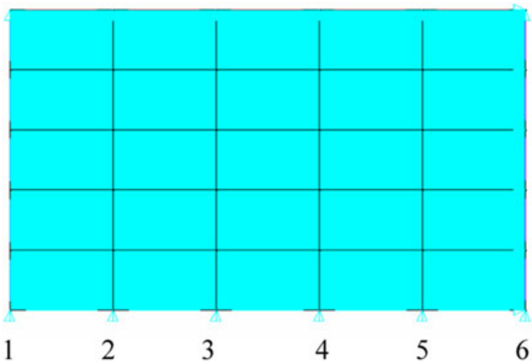

Fig. 6 Stress field simulation model denoted in Fig. 4 by using *dotted line*

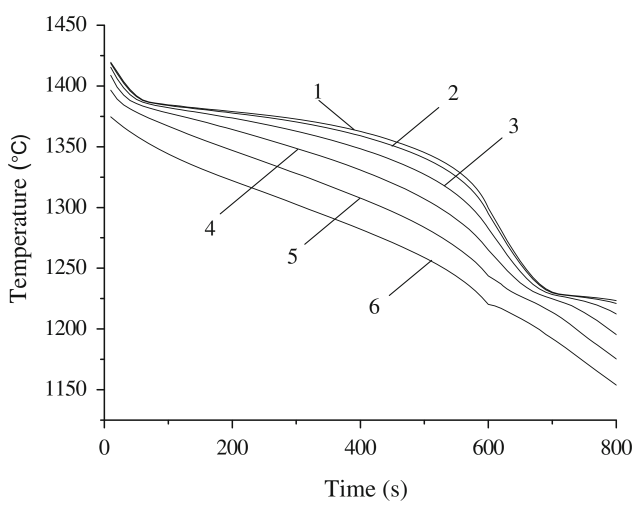

Fig. 7 Simulated temperature evolution at six points labeled in Fig. 5

4. Simulation Results

The simulated temperature results of the six points shown in Fig. 6 are displayed in Fig. 7, which was fitted by using the following equation:

$$T = a/[1 + \exp^{-(-b)(t-c)}] \quad \text{(Eq 10)}$$

where T is temperature, t is time, a, b, and c are parameters. The fitted parameters are listed in Table 6. The fitted functions were applied as the boundary conditions in the simulation of the stress-strain behaviors at elevated temperatures.

The simulated stress and strain results of the high chromium steel layer are shown in Fig. 8 and 9, respectively. It can be

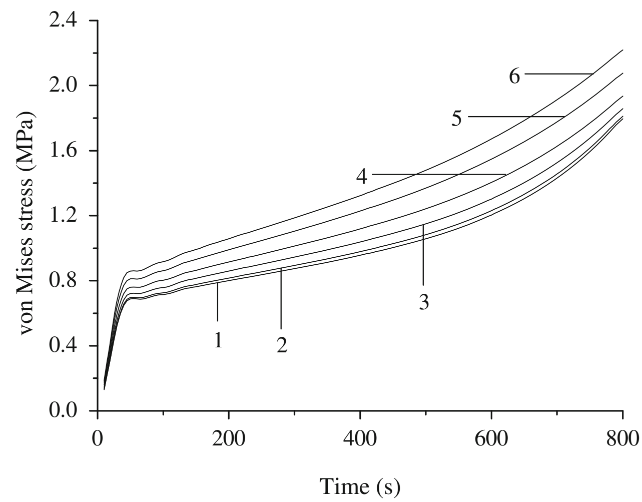

Fig. 8 Simulated evolution of von Mises stress at different points shown in Fig. 5

Table 6 Fitted parameters in Eq 8

	1	2	3	4	5	6
a	1412	1414	1422	1441	1480	1494
b	0.0037	0.0035	0.0030	0.0023	0.0017	0.0014
c	1253.4	1277.7	1349.6	1466.4	1609.5	1680.2

Table 4 Thermal physical properties of high chromium steel

T, °C:	20	200	400	600	800	1000	1200	1330	1334	1384	1390
ρ, kg/m^3	7740	7740	7740	7740	7740	7740	7740	7740	7740	7000	7000
C, J/kg · °C	500	503	543	560	580	585	590	590	2000	2000	590
λ, W/m^2 · °C	45.2	42.7	40	39	39	39	39	39	39	39	39

Table 5 Thermal physical properties of nodular cast iron

T, °C:	20	200	400	600	800	1000	1100	1334	1380
ρ, kg/m^3	7400	7400	7400	7400	7400	7400	7200	7200	7200
C, J/kg · °C	510	548	611	640	680	685	2750	2750	685
λ, W/m^2 · °C	31	31	29	29	29	29	29	29	29

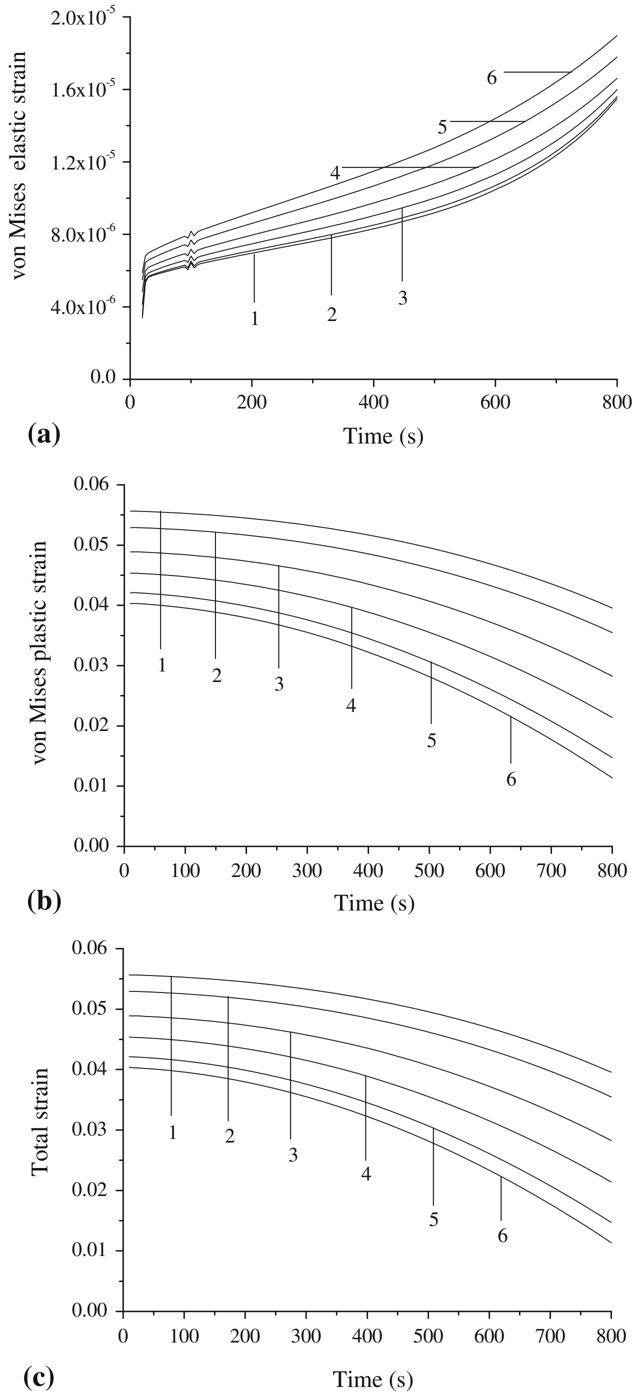

Fig. 9 Simulated evolution of (a) von Mises elastic strain, (b) von Mises plastic strain, and (c) total strain at six points shown in Fig. 5

seen that the von Mises stresses at each points are increased with increasing time. The temperature of the surface layer decreased more quickly than that of the inner layer, so the strength of surface layer is higher. Under the effect of centrifugal force, the von Mises stresses are increased from the inner part to the surface part as shown in Fig. 8. From Fig. 9, it can be seen that the amount of elastic deformation of the surface layer is greater than that of the inner one, while the amount of the plastic deformation is smaller than that of the inner one. The reason is that with a decrease in temperature, the elastic stain of metal is increased while the plastic stain is decreased as shown in Fig. 9(a) and (b). The plastic strain is much greater than the elastic strain of the high chromium layer at elevated temperatures as noted by comparing by comparing Fig. 9(a-c). Based on the isotropic hypothesis, because of the small von Mises strain and the low strength of the high chromium at elevated temperatures, the von Mises stresses are small and the maximum value is less than 2.4 MPa.

5. Conclusion

Based on the experimental results of thermomechanical compression test, the parameters of Anand model were determined. Then, the deformation processes at the strain rates of 1, 0.1, and 0.01 1/s were simulated by using FEM. The simulated and the experimental results are in good agreement, which indicates the correctness of the Anand model established in this work.

Unified viscoplastic Anand model was used to describe the constitutive behaviors of the high chromium steel at elevated temperatures, by which the stress-strain behaviors of centrifugal casting process at elevated temperatures were studied. The results show that the high-temperature deformation is mainly plastic one and the von Mises stress are very small, so the stresses introduced at elevated temperatures have little effect on the residual stress fields of steel pieces and the mechanical simulations of steel pieces using elastic-plastic model at low temperatures during cooling process are reasonable.

Acknowledgments

The author would like to express their gratitude for projects supported by Nature Science Foundation (E2004000238) of Hebei Province of China and Program for One Hundred Excellent Talents, Hebei Province of China.

References

1. A. Pramanik, L.C. Zhang, and J.A. Arsecularatne, Deformation Mechanisms of MMCs Under Indentation, *Compos. Sci. Technol.*, 2008, **68**, p 1304–1312
2. C. Vallellano, P.A. Cabanillas, and F.J. García-Lomas, Analysis of Deformations and Stresses in Flat Rolling of Wire, *J. Mater. Process. Tech.*, 2008, **195**, p 63–71
3. B. Gun, K.J. Laws, and M. Ferry, Elevated Temperature Flow Behaviour of a Mg-Based Bulk Metallic Glass, *Mater. Sci. Eng. A*, 2007, **471**, p 130–134
4. X.Q. Feng and D. Gross, Micromechanical Analysis of Microcrack-Induced Residual Strains in Quasi-Brittle Solids, *Comp. Mater. Sci.*, 1999, **16**, 362–371
5. X.L. Fu, Y. Li, and C.A. Schuh, Temperature, Strain Rate and Reinforcement Volume Fraction Dependence of Plastic Deformation in Metallic Glass Matrix Composites, *Acta Mater.*, 2007, **55**, p 3059–3071
6. L. Liu, Q. Chen, K.C. Chan, J.F. Wang, and G.K.H. Pang, The Effect of High Temperature Plastic Deformation on the Thermal Stability and Microstructure of Zr55Cu30Ni5Al10 Bulk Metallic Glass, *Mater. Sci. Eng. A*, 2007, **449–451**, p 949–953
7. B. Fedelich, A Microstructure Based Constitutive Model for the Mechanical Behavior at High Temperatures of Nickel-Base Single Crystal, *Comp. Mater. Sci.*, 1999, **16**, 248–258
8. S. Saxena and N. Ramakrishnan, A Comparison of Micro, Meso and Macroscale FEM Analysis of Ductile Fracture in a CT Specimen (Model I), *Comp. Mater. Sci.*, 2007, **39**, p 1–7

9. N.H. Zhang and M.L. Wang, Thermoviscoelastic Deformations of Functionally Graded Thin Plates, *Eur. J. Mech. A Solid*, 2007, **26**, p 872–886
10. A.A. Csontos and E.A. Starke, The Effect of Inhomogeneous Plastic Deformation on the Ductility and Fracture Behavior of Age Hardenable Aluminum Alloys, *Int. J. Plasticity*, 2005, **21**, p 1097–1118
11. S. Benke and D. Weichert, Thermo-Plasticity of Metal Foams, *Comp. Mater. Sci.*, 2005, **32**, p 268–275
12. R. Simões, A.M. Cunha, and W. Brostow, Computer Simulation of True Stress Development and Viscoelastic Behavior in Amorphous Polymeric Materials, *Comp. Mater. Sci.*, 2006, **36**, p 319–328
13. G.Z. Kang and Q.H. Kan, Constitutive Modeling for Uniaxial Time-Dependent Ratcheting of SS304 Stainless Steel, *Mech. Mater.*, 2007, **39**, p 488–499
14. B. Delibas, A. Arockiarajan, and W. Seemann, Rate Dependent Properties of Perovskite Type Tetragonal Piezoelectric Materials Using Micromechanical Model, *Int. J. Solid. Struct.*, 2006, **43**, p 697–712
15. Z.L. Zhang and J. Tong, A Study of Cyclic Plasticity and Viscoplasticity in a Newnickel-Based Superalloy Using Unified Constitutive Equations. Part II: Simulation of Cyclic Stress Relaxation, *Mech. Mater.*, 2007, **39**, p 73–80
16. J. Kang, D.S. Wilkinson, M. Jain, J.D. Embury, A.J. Beaudoin, S. Kim, R. Mishira, and A.K. Sachdev, On the Sequence of Inhomogeneous Deformation Processes Occurring During Tensile Deformation of Strip Cast AA5754, *Acta Mater.*, 2006, **54**, p 209–218
17. L. Anand, Constitutive Equations for the Rate-Dependent Deformation of Metals at Elevated Temperatures, *J. Engng. Mat. Tech.*, 1982, **104**, p 12
18. L. Anand, Constitutive Equations for Hot-Working of Metals, *Int. J. Plasticity*, 1985, **1**, p 213–231
19. L. Anand and S. Brown, Constitutive Equations for Large Deformations of Metals at High Temperatures, *Constitutive Models of Deformation*, J. Chandra and R.P. Srivastav, Eds., SIAM Press, Philadelphia, 1987